Elastic seismic inversion and reservoir characterization in the Llanos Basin, Colombia

MIGUEL BOSCH. Universidad Central de Venezuela Diego Morales, Yohaney Gomez, Thais Kazmierczak, Trino Salinas, and Gabriel Álvarez, Pacific Rubiales Energy Adriana Moreno, Youleissy Pino, and Edinson Medina, Info Geosciences Technology and Services

Abstract

The contribution of seismic inversion to lithology and fluid characterization in oil reservoirs is geology and data dependent. Several studies of reservoir characterization based on elastic seismic inversion in the Llanos Basin in Colombia have proved to be successful for accurate description of the siliciclastic lithology of lower members of the Carbonera Formation. Mass density estimated from the inversion has been an important lithology discriminator because of compaction of shale, which exhibits larger densities than sand. In the analysis of properties calculated from well-log data, the separation in property space of oil sands and brine sands is moderate to small. Oil sands likely are distributed toward the zones of lower V_p/V_s ratio, Poisson's ratio, density, and bulk modulus, compared with other lithofluid types. The theoretical effect of fluid substitution in elastic rock parameters and density, although small because of the proximity of heavy-oil density to water density, is nevertheless present in these reservoirs. Successful exploitation of the seismic information associated with the discrimination of oil-bearing and brinebearing sands has been achieved via fine calibration of the elastic inversion and derived reservoir indicators and by combining this information with relative two-way time (TWT) location of the strata to interpreted horizons. With statistical analysis and direct analysis over crossplots, indicators for oil sands have been formulated that are consistent with information available from wells, although slightly less accurate than lithologic (V_{shale}) estimation. After lithology estimation is performed from the seismic-inversion results, further improvement of the lithology description is achieved by combining the seismic-derived lithology with the localized well-log lithology profiles using geostatistical methods.

Introduction

The analysis of seismic-reflection amplitudes provides a description of the elastic behavior of the propagation medium and particularly allows estimation of the strata elastic parameters in sedimentary basins. The accuracy of the estimation depends on various factors such as source energy, offset range, energy penetration, attenuation, target depth, and others. Some of those factors are influenced by the specific geologic configuration of the area. On the other hand, the possibility of discriminating lithology or fluids or estimating porosity from the elastic description of the medium depends largely on the characteristics of the target formation, which determines the particular property relationships between reservoir and elastic parameters. For all those reasons, the objectives that can be reached via seismic-inversion analysis depend highly on the area and the available data set.

The Llanos Basin, in Colombia, is a wide area at the northeast of the country that hosts prolific oil-producing fields. Oil reservoirs are located commonly in the deepest members of the Carbonera Formation, typically at the C7 (basal sands) and C5B levels. The stratigraphic setting corresponds to deltaic and fluvial environment, reworked through extensional tectonics. Sand bodies are of good quality in general but are highly heterogeneous and complex in morphology. Oil traps result from a combination of stratigraphic and structural features, with stratigraphic predominance. For the optimal exploitation of oil fields, a 3D description of the lithology is critical, particularly to drive horizontal drilling. Horizontal wells have been a key resource to increase production in Llanos Basin fields.

We have carried out various studies of seismic elastic inversion with data from the Llanos Basin that include reservoir characterization based on the estimated elastic configuration of the medium. Those studies show successful results in accurate lithology description for the stratigraphic level of the producing members of the Carbonera Formation. In addition, we have found that seismic data are sensitive to pore fluid (oil-brine), although the seismic effects associated with fluids are small compared with superposed porosity and lithology effects. We have exploited this seismic information with fine calibration against well-log data to develop probability indicators of the presence of oil sands that correlate with well information.

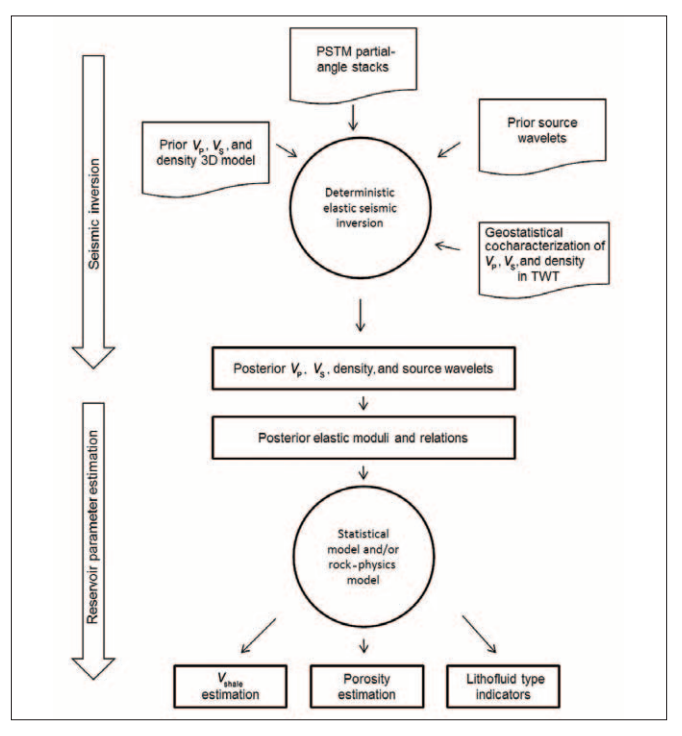


Figure 1. Basic information and process flow for the consecutive steps of seismic elastic inversion and reservoir parameter estimation.

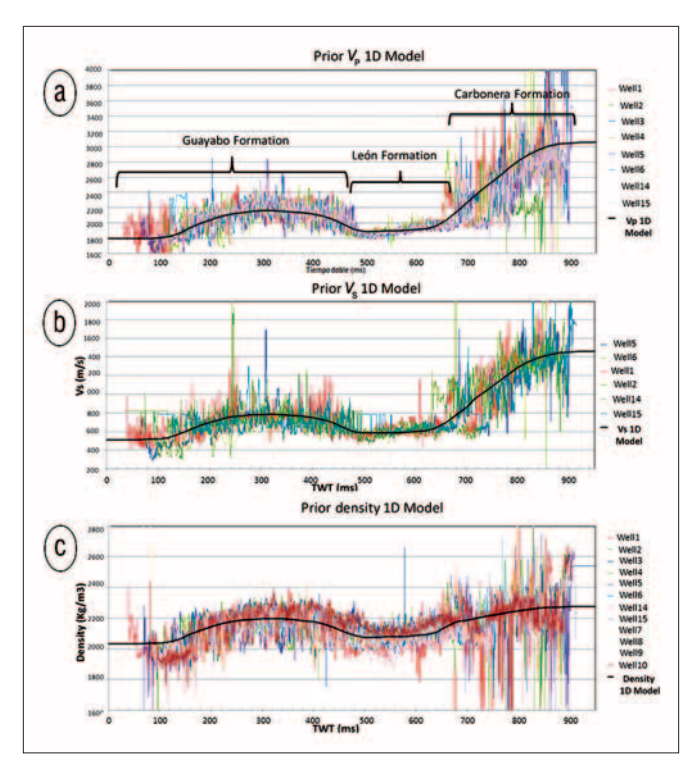


Figure 2. (a) $V_{\rm p}$, (b) $V_{\rm s}$, and (c) density profiles (colored lines) calculated from well logs in an area of the Llanos Basin against TWT after correction to a common horizon time location. The smooth trend for $V_{\rm p}$, $V_{\rm g}$, and density (black line) is used to build up the 3D prior model after extrapolation along interpreted horizons.

Oil production in the Llanos Basin is also obtained in some cases from the C3 member of the Carbonera Formation and from various Cretaceous formations in the central area of the basin. Those members and formations are not within the scope of the present work, which pertains to the lowest members of the Carbonera Formation (C5B through C7).

Methods for seismic inversion and reservoir parameter estimation

The inversion methodology we have applied is based on seismic modeling of several partial-incidence angle stacks after prestack time migration (PSTM). The modeling is performed by solution of PP reflectivity with Zoeppritz equations for the elastic isotropic medium, parameterized in layers in two-way time (TWT) domain, and convolution with seismic wavelet functions. The inversion approach is deterministic by minimization of a combined objective function (data deviations + priors deviations),

$$f(\mathbf{m}, \mathbf{s}) = (\mathbf{d} - \mathbf{d}_{obs})^{T} \mathbf{C}_{d}^{-1} (\mathbf{d} - \mathbf{d}_{obs})$$
Seismic data misfit
$$+ (\mathbf{m} - \mathbf{m}_{prior})^{T} \mathbf{C}_{m}^{-1} (\mathbf{m} - \mathbf{m}_{prior}) + (\mathbf{s} - \mathbf{s}_{prior})^{T} \mathbf{C}_{s}^{-1} (\mathbf{s} - \mathbf{s}_{prior}).$$

Medium property deviations from the prior Source-parameter deviations from the prior

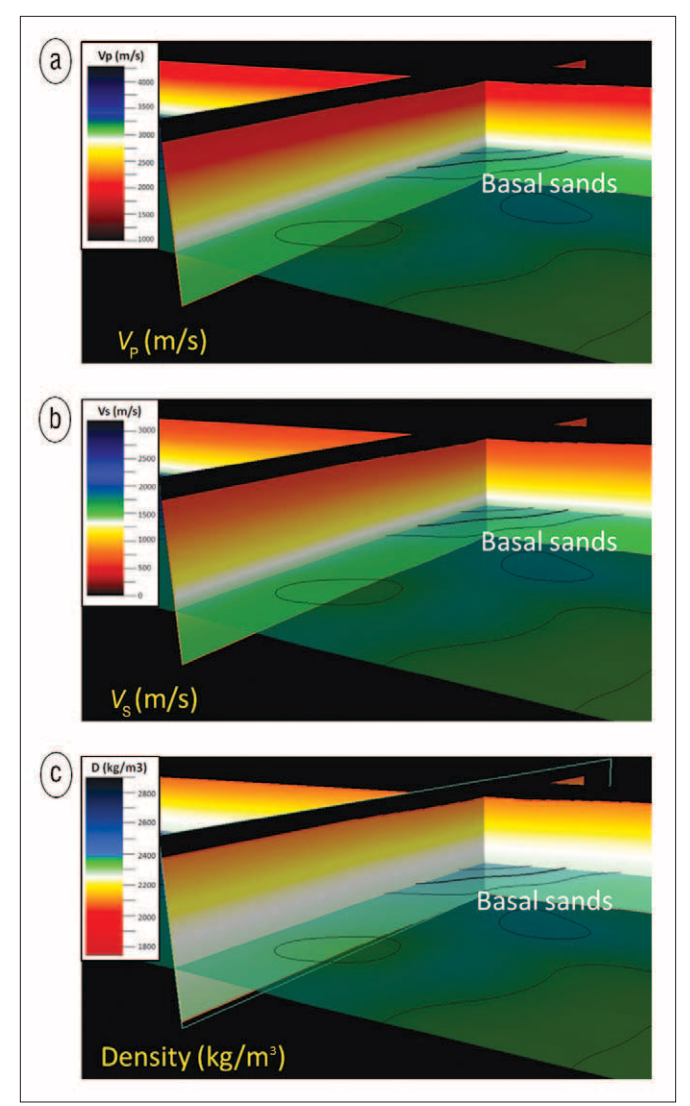


Figure 3. Sections of (a) V_p , (b) V_s , and (c) density prior 3D models following the top of basal sands (C7) and the 1D area trend shown in Figure 2.

Above, **d**, **m**, and **s** represent modeled seismic data, elastic-medium configuration, and source parameter arrays, respectively; \mathbf{d}_{obs} is the observed seismic data array; $\mathbf{m}_{\text{prior}}$ and $\mathbf{s}_{\text{prior}}$ are prior configurations of the elastic properties and source wavelets; and \mathbf{C}_{d} , \mathbf{C}_{m} , and \mathbf{C}_{s} are data, property, and source-parameter covariance, respectively.

The method includes (1) joint estimation of seismic compressional velocity, seismic shear velocity, mass density, and source wavelet deviations from the priors; (2) prior smooth configuration of the properties for the medium based on well-log and seismic-horizon information; (3) prior information about the vertical geostatistical characterization of the medium properties based on well-log data; and (4) prior source wavelets for each incidence angle stack. The objective function is minimized via iterative linearization of the forward problem using a Gauss-Newton technique. Figure 1 shows a flow diagram of our inversion approach.

After the isotropic elastic-medium parameters are estimated by seismic inversion, we proceed with the estimation of reservoir parameters (lithology, porosity, and reservoir oil-bearing

sand probability) based on characterization of their relationship with the elastic properties and mass density. We combine for this purpose statistical analysis and rock-physics models depending on the actual success of the indicators compared with welllog information. We have used with success (1) direct characterization and modeling by inspection of crossplots, (2) calibration of rock-physics functions against property data, (3) linear regression, and (4) discriminant analysis. We validate the adopted models at the level of well-log and elastic-inversion-estimated properties against lithology, porosity, and fluid content evaluated with well-log information. A review of inversion approaches for reservoir description and discussion

on some of the components used here can be found in Bosch et al. (2010).

In the Llanos Basin, we have not attempted a unified petrophysical-geophysical inversion approach because rockphysics relationships have important vertical changes across the Carbonera Formation as a result of shale compaction in the lower members. Thus, the rock-physics characterization we use for estimation of reservoir parameters is specific to the target strata, C7 or C5B, depending on the location within the Llanos Basin. First we infer the elastic parameters and mass density within a large time window for a full picture of the Carbonera Formation and the underlying basement, and then we attempt to infer lithology and fluid indicators for a smaller time window comprising the target strata.

Seismic inversion

We use a smooth prior model for $V_{\rm p}$, $V_{\rm S}$, and density based on a compilation of information from well-log data. An example is shown in Figure 2, which displays well logs for mass density, V_p , and V_s in a typical Llanos area and a common multispline model that follows the long-period trend of the properties. For this plot, well-log data are correlated in time to a common well location according to appropriate seismic horizons. The 3D prior property model is extrapolated from the 1D common trend following the reference-interpreted seismic horizons. Figure 3 shows prior property models.

Carbonera target levels are relatively shallow, between 800 ms and 1000 ms TWT for the areas studied, and penetration of high frequencies is good when explosive sources are used. The common processing sequence we recommend is basic, including predictive or spiking deconvolution, surface-consistent amplitude recovery, and prestack time migration. Dominant frequency at the target level is within the range of 80 to 120 Hz. By the criterion of a quarter dominant period, we achieve in most cases a property-model resolution of 2 ms, the same as the seismic sampling interval. As a complement to a simple processing sequence, we are encouraged to carry on more

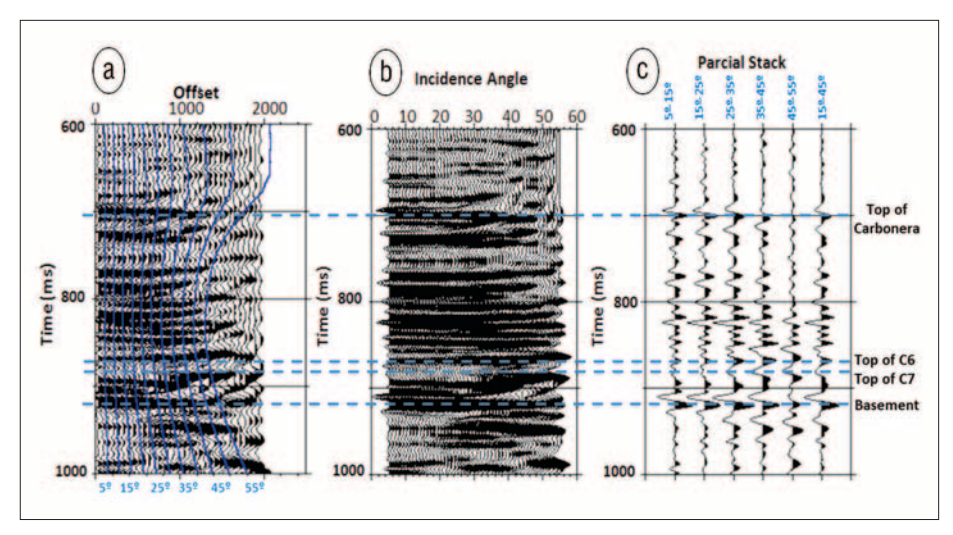


Figure 4. Example of a PSTM CDP gather (a) in offset domain with lines indicating the incidence angle dependence with offset and (b) after transformation to incidence-angle domain and (c) partial stacks at selected incidence-angle ranges: 5° to 15°, 15° to 25°, 25° to 35°, 35° to 45°, and 15° to 45°.

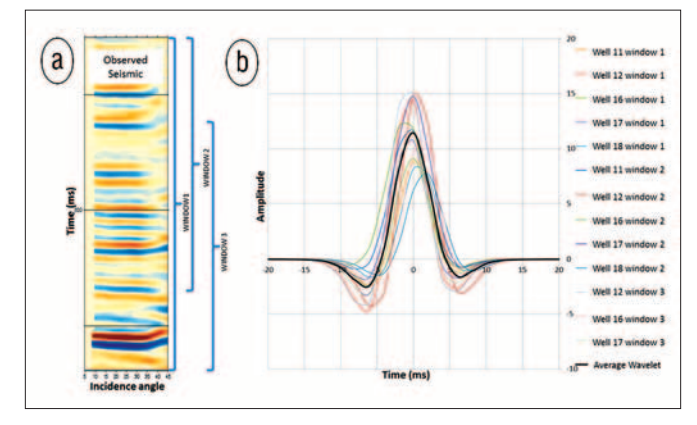


Figure 5. (a) Seismic PSTM gather at a well location and (b) various source wavelets (colored lines) estimated for several well locations and time windows at the level of the Carbonera Formation and basement reflections. The average source wavelet (black line) is used as the prior wavelet for the elastic seismic-inversion process.

elaborated processing strategies (such as advanced migration algorithms, moderate frequency enhancement, interpolation, and so forth) that can contribute to seismic-imaging improvement while respecting reflectivity amplitudes — always having a close interaction with the interpreters for quality control.

Figure 4 shows a typical CDP offset gather after PSTM and its incidence-angle mapping. In this case, we have partially stacked traces within 10° incidence-angle bins, starting at 5° to 55°. The angle coverage is dependent on the geometry of acquisition. For standard geometries, the smallest and largest of the angle bins commonly are subjected to spatial nonhomogeneous fold of coverage generating acquisition-amplitude footprint effects. This commonly has been the situation for partial stacks with the smallest angle (5-15°) and largest angle (45-55°). After testing, we have found better results excluding the extreme short and extreme large angle-range bins and retaining as input for the inversion the better spatially sampled small (15-25°), medium (25-35°), and large (35–45°) incidence-angle partial stacks.

We estimate the source wavelet in three steps:

- standard seismic modeling from impedance well logs for well-to-seismic matching and approximate assessment of the frequency and phase source wavelet
- stochastic modeling of the source wavelet against PSTM gathers for further adjustment of wavelet shape and angle dependency
- 3) final adjustments of source-wavelet deviations in the seismic-inversion process estimated jointly with V_p , V_s , and density on a CDP-per-CDP base, to assess spatial variation of the source wavelet

Figure 5 shows a CDP PSTM gather and various wavelets estimated via stochastic analysis for various well locations and time windows, as mentioned in item 2 above. In this particular case, we did not need to consider a variation of the wavelet with the incidence-angle ranges. Figure 5 also shows an average wavelet which is the prior source wavelet for the inversion, step 3 in the sequence.

The prior property model is adjusted in iterative steps through inversion to estimate strataproperty (V_p , V_s , and density) deviations from the prior that explain the seismic reflections at various partial-angle stacks. Figure 6 shows a detail of the observed, calculated, and difference (residual) incidence angles of the seismic partial stacks. Figure 7 shows the corresponding estimate of the strata mass density, V_p , and V_s . As previously explained, the inversion jointly estimates deviations of source wavelets for each partial-angle stack and CDP. Figure 8 shows an

example of the prior, final, and difference source wavelets along an inline section through the volume.

Lithology characterization

One major objective of the inversion is lithology inference; we have already mentioned the importance of 3D mapping of sand bodies for horizontal-well locations in the Llanos Basin. The basin's siliciclastic Carbonera Formation lithology is described by shale volume fraction ($V_{\rm shale}$). At the lower (older) members, we have found a good relationship between mass density and $V_{\rm shale}$. Because of shale compaction, shales have larger mass density than sands. Figure 9 shows an illustration of this relationship based on well logs for various

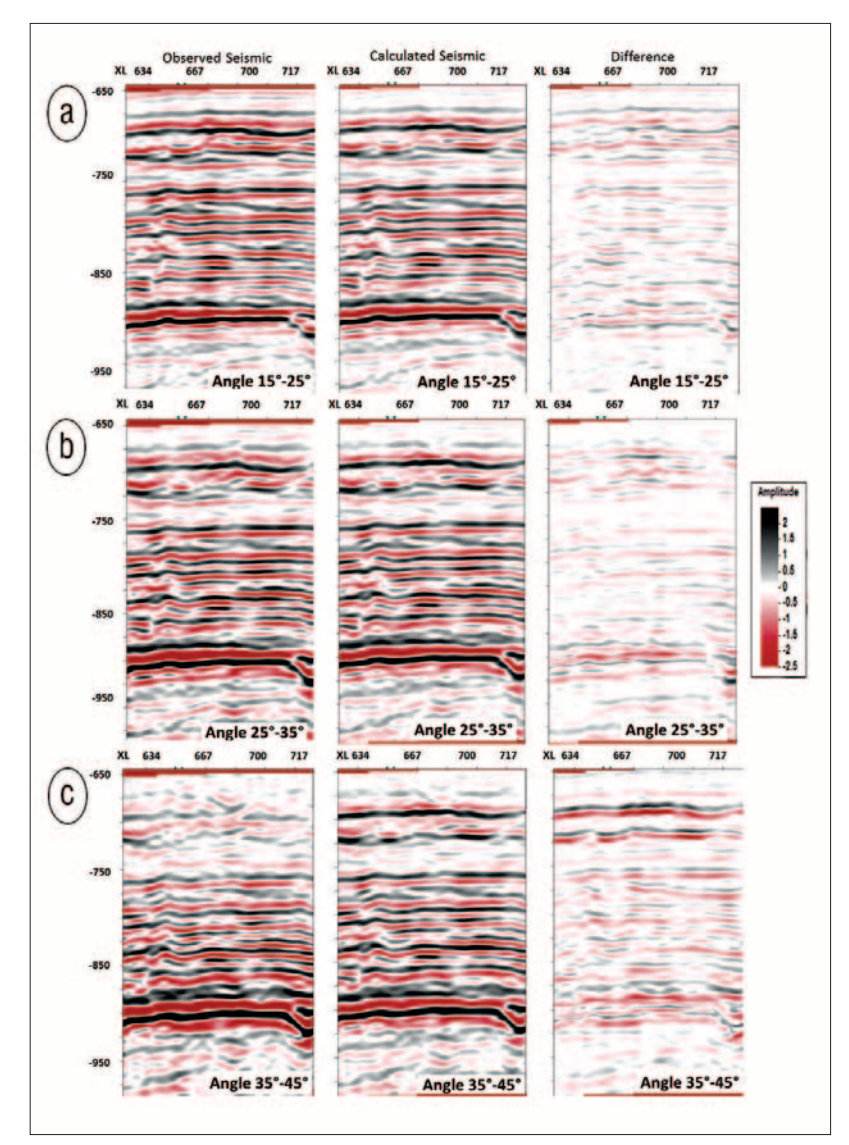


Figure 6. Observed, calculated, and residual incidence-angle partial stacks for incidence-angle ranges of (a) 15° to 25°, (b) 25° to 35°, and (c) 35° to 45°.

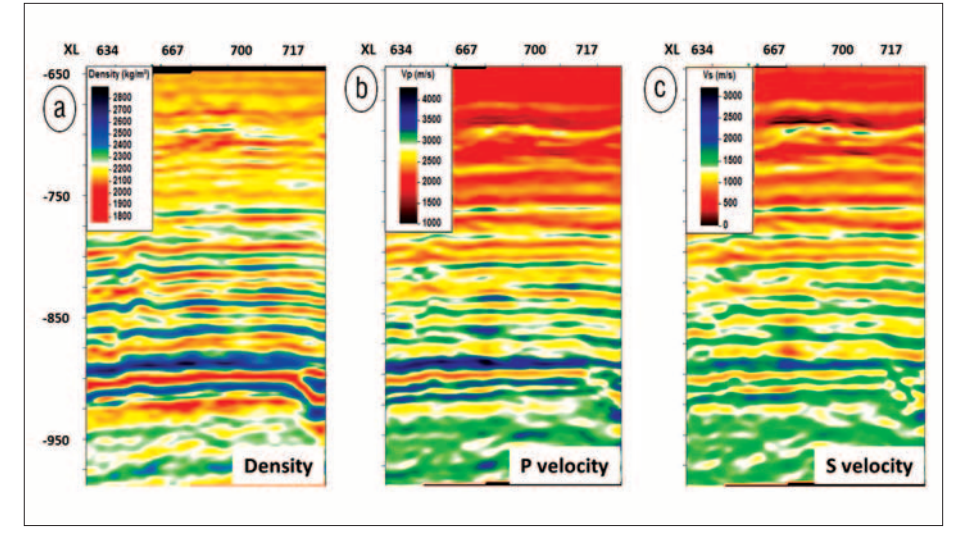


Figure 7. (a) Mass density, (b) $V_{\rm p}$, and (c) $V_{\rm s}$ estimated by elastic inversion for the same seismic data section shown in Figure 6.

wells at C6 and C7 levels. The correlation factor between density and $V_{
m shale}$ is 0.7 in these well-log-derived data.

We have explored other relationships and multivariate predictions. However, the best estimation of a seismic $V_{\rm shale}$ has been obtained with direct linear regression from the mass density inferred from seismic inversion after a logarithmic transformation of the shale volume factor.

Figure 10a shows a section of the $V_{\rm shale}$ estimator and the corresponding V_{shale} profile derived from well-log data at an example well. We found good correlations between the $V_{\mbox{\scriptsize shale}}$ estimator derived from the inversion study and the well-log data, with a correlation factor of the order of 0.8 on large sets of control wells (more than 20) distributed across large seismic-survey areas (more than 250 km²). Our statistics clearly show that lithology prediction based on prestack seismic-reflection data for the Llanos basal Carbonera sand formation is successful.

Figure 10b shows the $V_{\rm shale}$ estimation and two horizontal wells successfully drilled through the producing basal sand strata. The resistivity log is plotted to the side of the well path, showing a good correlation between the oil-related increase of resistivity and the quality of the top

basal sands — as inferred from the low shale fraction estimated from seismic inversion.

Total-porosity characterization

We have applied various statistical procedures for the prediction of total porosity. One of the approaches is linear multivariate regression from various elastic moduli and

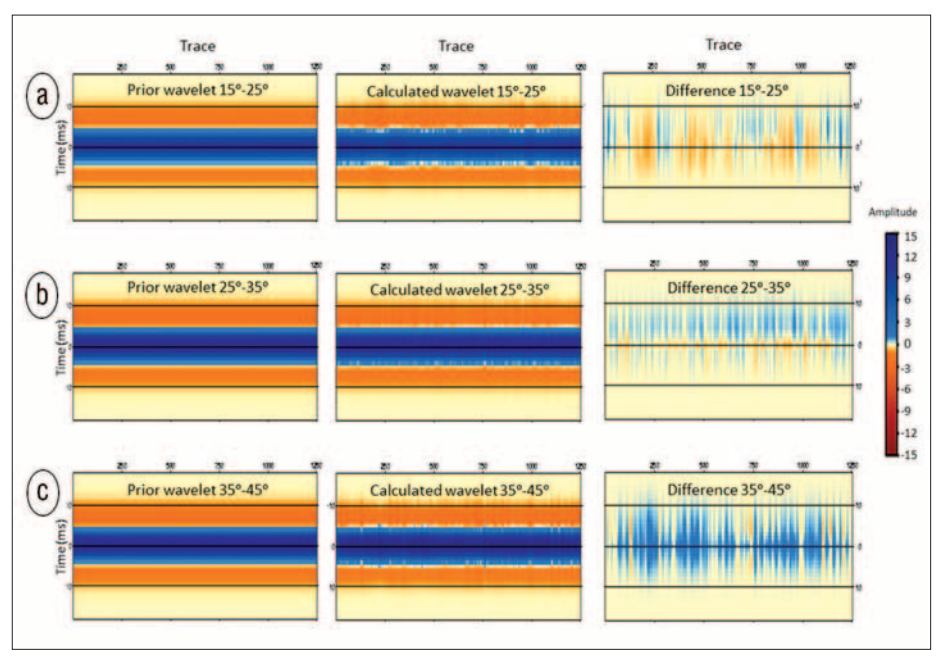


Figure 8. Prior source wavelet, calculated source wavelet, and their difference for each incidence-angle partial stack along an inline through the data volume: (a) 15° to 25°, (b) 25° to 35°, and (c) 35° to 45°.

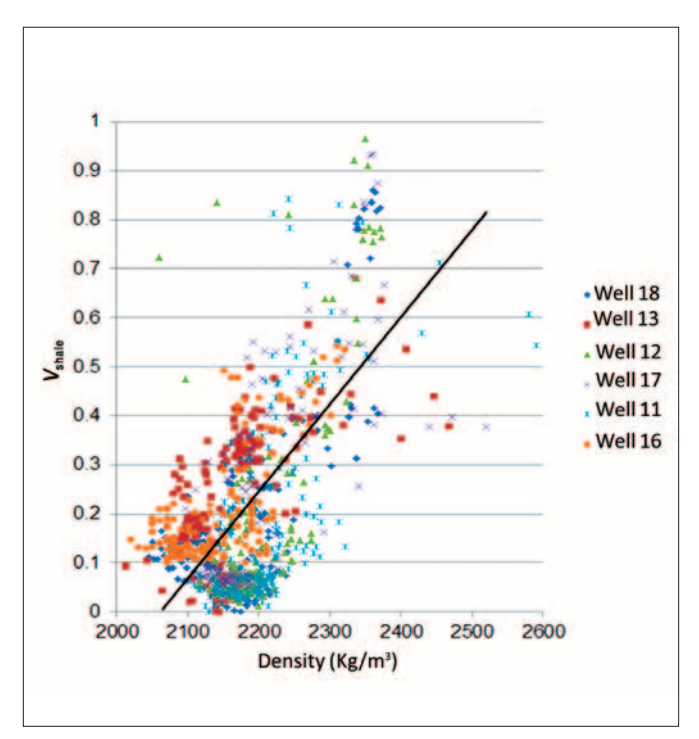


Figure 9. Mass density and shale volume fraction data calculated from well logs at the levels of the C6 and C7 Carbonera Formation members. The correlation factor in these data is 0.7.

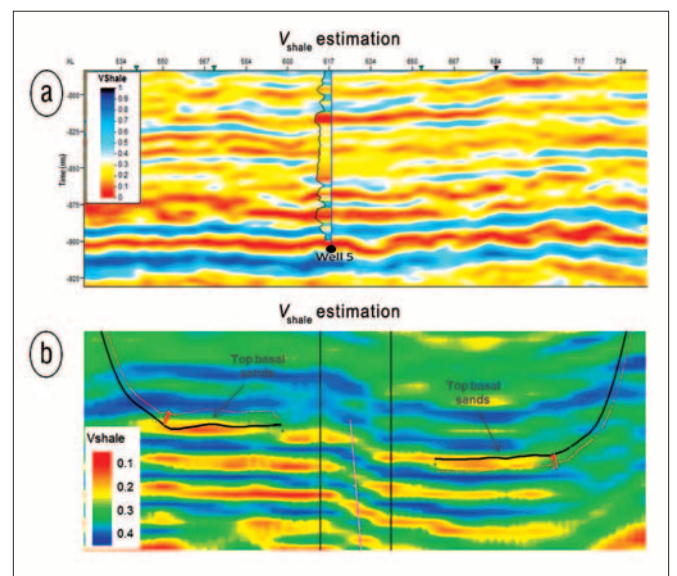


Figure 10. (a) V_{shale} derived from seismic inversion and a V_{shale} profile calculated from well-log data for a vertical well. Well-to-seismic V_{shale} estimation is of 0.8 correlation factor in average over the 17 control wells in this area. (b) V_{shale} derived from seismic inversion and horizontal well paths drilled with successful arrival in the oil-bearing sand stratum. The black line shows the trajectory to the wells, and the red line to the side of the trajectory is a resistivity log. Notice that oil-associated increase in resistivity has good correlation with the estimated quality of the top basal sands.

mass density. Figure 11a, based on a different seismic data set than Figure 10, shows a section of total porosity derived from inversion with a 0.8 correlation factor with well-log information, obtained via multivariate linear regression. Another approach is calibration with well-log data of simple rock-physics relations, such as the relation of density to porosity and the relation of Wyllie slowness to porosity and their combination.

Oil-bearing sand characterization

Oil in the Llanos Basin is of heavy or medium API gravity; its mass density and acoustic properties have small deviations from the corresponding brine properties. Because of this deviation in elastic properties, there is a direct seismic-reflectivity effect of the fluids in the pores for the basal Carbonera Formation, although small compared with lithology and porosity effects. However, depending on the area, seismic data quality, and appropriate seismic data to well-log calibration, the fluid information imprinted in seismic reflections can be exploited. In general, oil-bearing basal sands at C7 are more likely to be distributed in the zone of low mass density, low $V_{\rm p}/V_{\rm s}$ ratio, low Poisson's ratio, and low bulk modulus than the corresponding brine-bearing sands.

Figure 12 shows an example of crossplots of oil-bearing sands, brine-bearing sands, and shaley sands corresponding to Carbonera C6 and C7 members with property data calculated from well logs (Figure 12a), a fluid-substitution model (Figure 12b), and seismic inversion (Figure 12c). Although significant overlap of lithotype support in the crossplots is

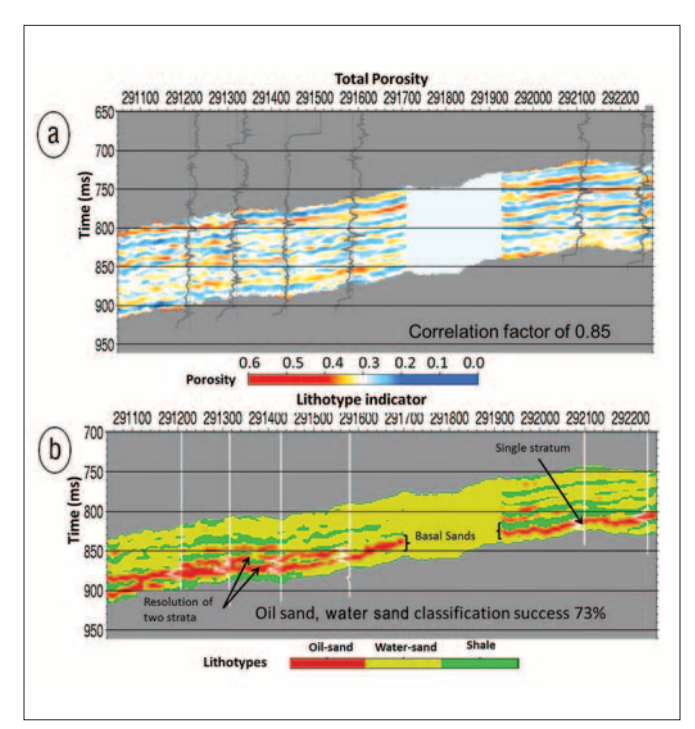


Figure 11. (a) Total porosity estimated from seismic inversion and porosity profiles from well logs. Well-to-seismic porosity estimation is of 0.8 correlation factor in this area. (b) Most likely lithotypes obtained from probability densities defined in a discriminant space resulting from the linear combination of elastic parameters for oil sand, brine sand, and shale. The discrimination also includes TWT relative to the top of target stratum C7. This image is not from the same data set as previous figures.

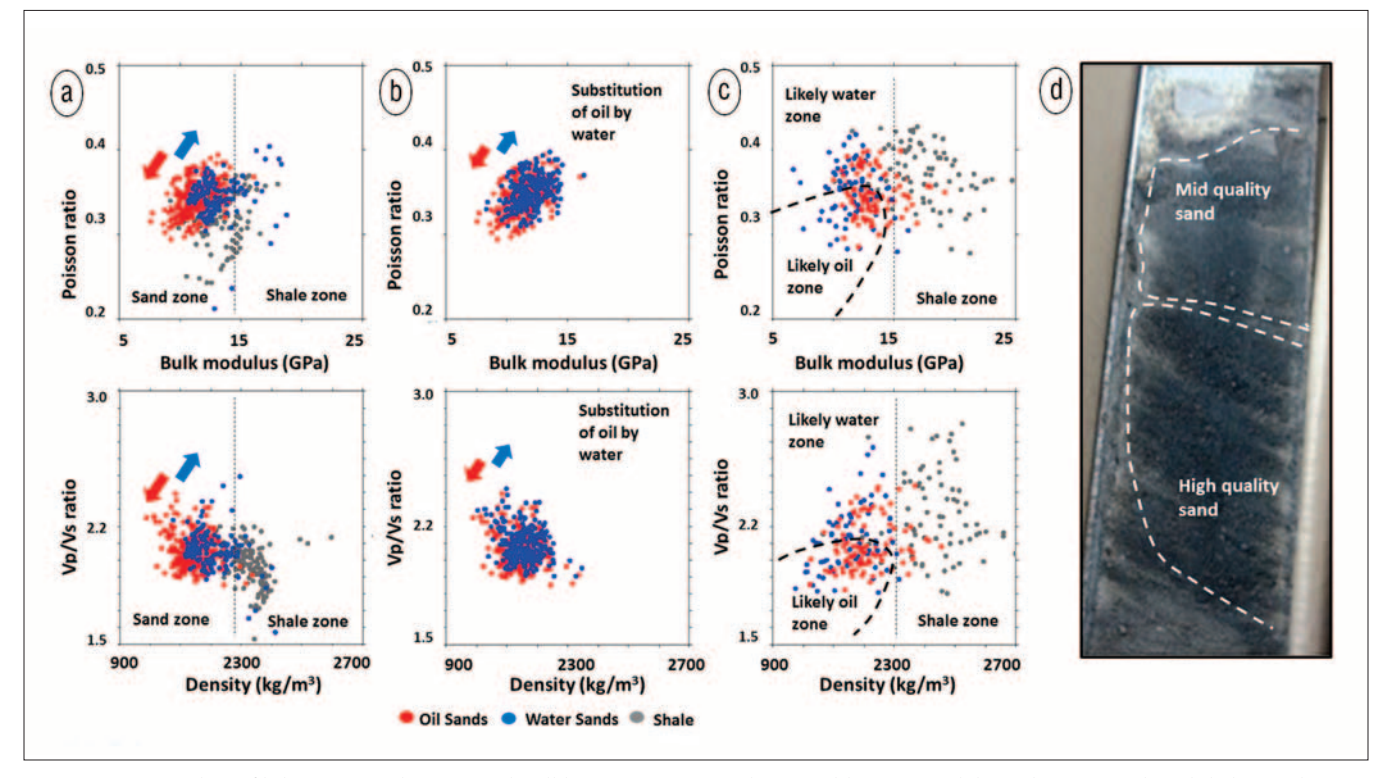


Figure 12. Crossplots of lithotype samples in several well locations corresponding to oil-bearing sand, brine-bearing sand, and shaley sand, according to (a) well-log-derived properties, (b) a fluid-substitution model, and (c) seismic-inversion-derived properties. In the fluid-substitution case, water-sand samples (blue) are modeled from the oil-sand samples (red) of part (a). (d) Photographic image of a core sample from C7 oil-bearing sand showing porosity heterogeneity.

shown, there are higher probabilities for oil in pores in the indicated lower areas of the crossplots.

The fluid-substitution exercise (Figure 12b) shows the direction of displacement of rock properties caused by fluid change, in agreement with that observed in the crossplots of welllog data. Note that fluid substitution based on the Gassmann model (Mavko et al., 2003) does not fully account for the size of property displacements shown in the well-log-derived data. We think the fluid effect might be reinforced by associated frame and pore effects, such as larger permeability of oil-bearing sands or better preservation of pore space after migration in oil sands compared with brine sands.

Figure 12d illustrates heterogeneity in porosity of basal sands. Heavy-oil saturation is associated with preference to high-quality sands, which are characterized by larger porosity and permeability.

We have exploited the small to moderate fluid effect in properties and reflectivity by the construction of lithotype probability indicators, using two methods: (1) on direct selection at the elastic parameter and mass density space and (2) in discriminant space after discriminant analysis. For those indicators, we combine the information on property distribution of the oil-sand lithotype with probabilities associated with the location of the C7 target sands within the appropriate time window and the related interpreted time horizon for stratum-formation specificity of the indicator. In both cases (direct or discriminant space), we have obtained coherent results of the oil-sand indicator against well-log data with a correlation factor to well-log information that ranges between 0.7 and 0.6, depending on area and data quality.

Figure 11b, from a different seismic data set than the one shown in Figure 10, shows lithotype indicators derived from the discriminant-analysis approach. The indicator is superposed to saturation profiles derived from well-log data showing assertive correlation for the oil-bearing sand strata and their levels — two levels at the right-hand side of the figure — with a correlation of 0.7 to oil saturation.

Figure 13a (from the same data set shown in Figure 10) shows probabilities for oil sands based on probability densities directly selected from analysis of property crossplots, which has a correlation of 0.6 with oil saturation at 17 control wells in the area. Figure 13b shows probabilities for oil-bearing sands obtained with a discriminant-analysis approach with similar correlation to well-log information. Figure 13c shows the most likely lithotype derived from discriminant analysis.

Maps and geostatistics

Based on vertical integration of the $V_{\rm shale}$ estimator and probabilities for oil sands, various types of maps are produced.

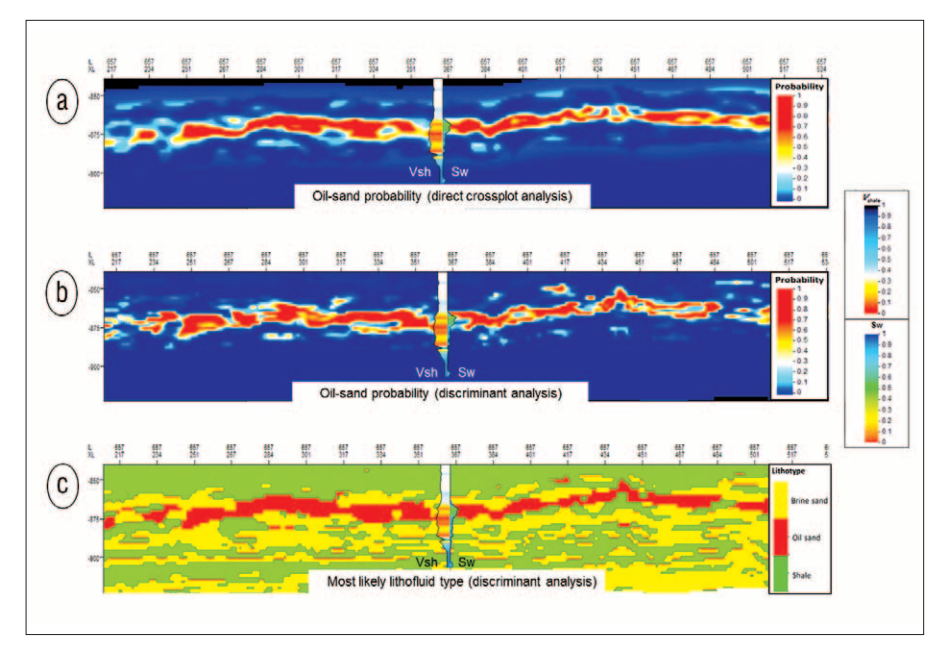


Figure 13. Well-log-derived $V_{\rm shale}$ and water-saturation profiles superposed to oil-sand probabilities calculated from the results of elastic inversion and based on (a) direct characterization in the space of properties and (b) discriminant analysis. (c) Most likely lithofluid types inferred via discriminant analysis based on the results of inversion. In all cases, TWT information relative to the top of the target stratum C7 is included.

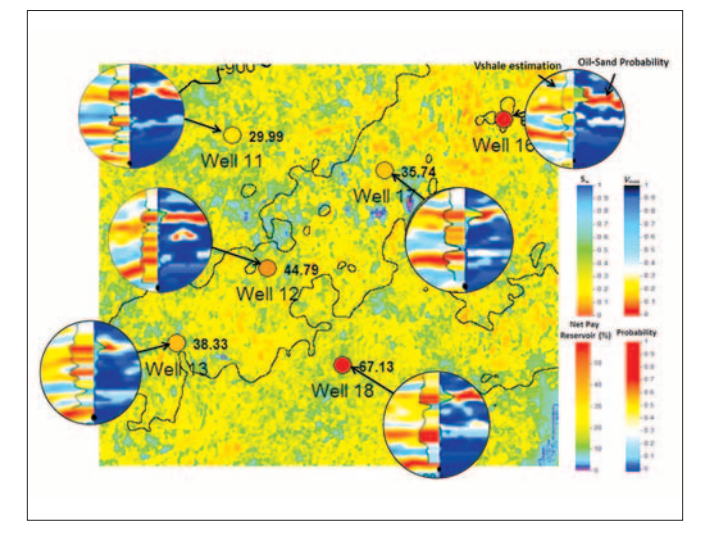


Figure 14. Map of net-pay-to-gross ratio for C7 sand with superposition of values calculated from well data at six locations. The overall correlation factor over 17 control wells in the area is of 0.7. Circular plots show for each well location the seismic-derived $V_{\rm shale}$ estimator, the probability for oil sand, $S_{\rm w}$, and $V_{\rm shale}$ according to well-log data.

Figure 14 shows an area with net-pay-to-gross calculations and comparison to well-log data with overall correlation of 0.7.

Spatial horizontal sampling available through the seismic-derived lithology and lithotype estimators can be used for geostatistical characterization of the horizontal variability of $V_{\rm shale}$ and saturation. Figure 15 shows an image of C7, with the empirical and modeled standardized variogram. The variogram shows ranges for sand bodies of approximately 2 km with an exponential variogram that displays the known

morphological heterogeneity of sand distribution. Combination of the seismic $V_{\rm shale}$ estimator with well-log data via geostatistical methods, such as cokriging, improves the precision of 3D estimation of sand bodies.

Figure 16 shows a slice through the Carbonera C7 $V_{\rm shale}$ seismic estimator and the resulting update obtained by combination of the $V_{\rm shale}$ seismic estimator with the well-log $V_{\rm shale}$ at well locations using a cokriging strategy. By construction, the updated result shown in Figure 16b honors the well-log lithology at well locations.

Conclusions

Combination of seismic elastic inversion and statistical rock-physics reservoir-property estimation is useful in the Llanos Basin for providing an accurate description of lithology at the Carbonera Formation, particularly for the estimation of shale volume fraction in three dimensions, which is important for development of the producing fields via horizontal drilling. Further combination in three dimensions with localized well-log information via geostatistical tools improves the accuracy of the sand model.

In our studies at the Llanos Basin, mass density is an important parameter for lithology description because of its correlation with the shale volume fraction in Carbonera basal sands (C7). This behavior is also shown at the lowest strata of C5. In addition, total porosity can be estimated successfully from elastic parameters and mass density inferred from elastic inversion. The direct effect of oil-brine substitution in sandstone pores, although small because of the density of heavy oil, can be exploited by means of fine calibration and horizon interpretation to develop oil-bearing sand-probability fields and most likely lithotype fields that are coherent in reproducing well-log information. Oil-bearing sands, although with significant support overlap, are more likely to be of lower mass density, lower $V_{\rm p}/V_{\rm s}$ ratio, lower bulk modulus, and lower Poisson's ratio than brine-bearing sands, as expected by rock-physics modeling. **TLE**

References

Bosch, M., T. Mukerji, and E. F. Gonzalez, 2010, Seismic inversion for reservoir properties combining statistical rock physics and geostatistics: A review: Geophysics, **75**, no. 5, 75A165–75A176, http://dx.doi.org/10.1190/1.3478209.

Mavko, G., T. Mukerji, and J. Dvorkin, 2003, The rock physics hand-book, 2nd ed.: Cambridge University Press.

Acknowledgments: We thank Pacific Rubiales Energy and Info Geosciences Technology and Services for their authorization to publish the data shown in this article.

Corresponding author: miguel.bosch@ucv.ve

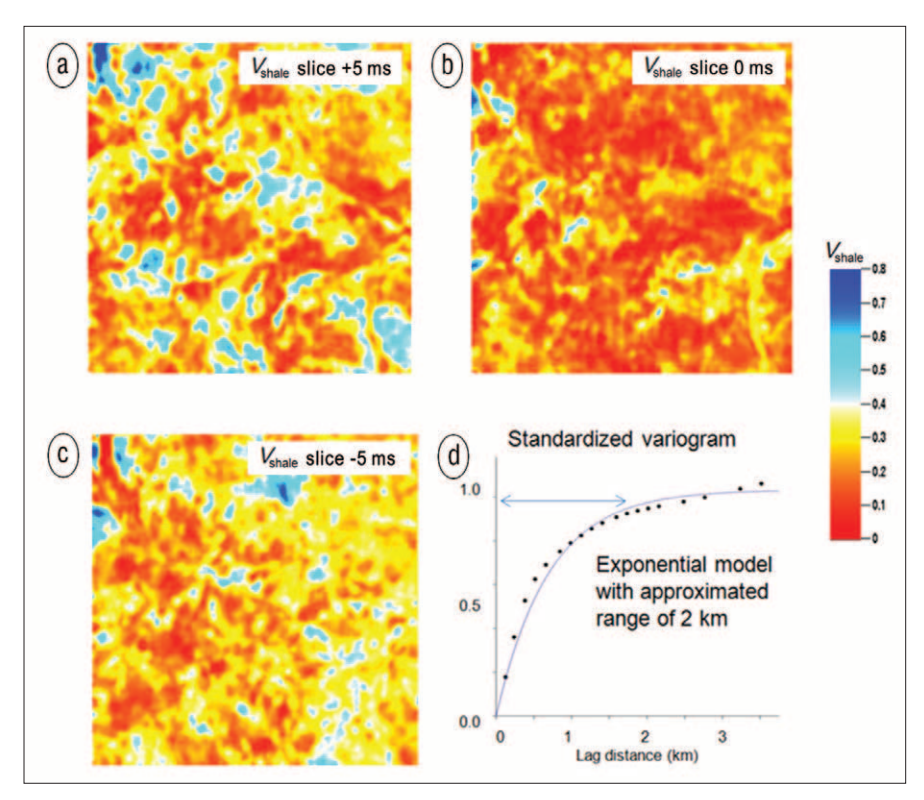


Figure 15. (a through c) Parallel horizon slices through the seismic estimator of $V_{\rm shale}$ at the center of the C7 sand strata. (d) The corresponding empirical (dots) and modeled (continuous line) spatial semivariogram.

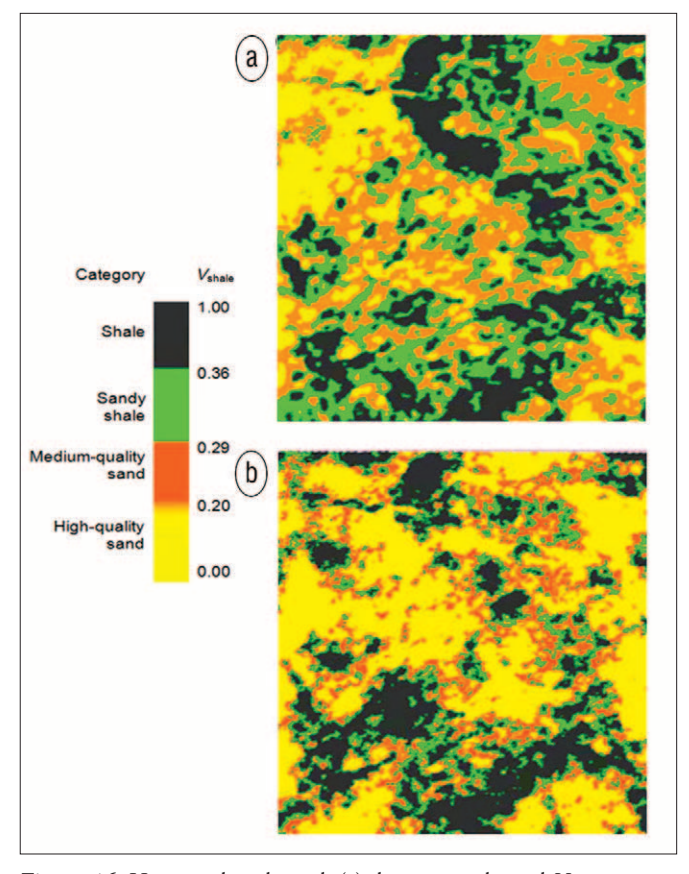


Figure 16. Horizon slice through (a) the seismic-derived V_{shale} estimator and (b) the seismic-derived V_{shale} estimator after combination with the localized well-log information on V_{shale} by cokriging.